

Simultaneous measurement of temperature and flow field formed by a small heated sphere in water by near-infrared absorption imaging method and particle tracking velocimetry

by Zhenlei. Wang*, Yuki. Arakawa *, Van Cuong Han*, Katsuya Kondo**, Naoto Kakuta*

*Department of Mechanical Systems Engineering, Tokyo Metropolitan University, 1-1 Minami-Osawa, Hachioji, Tokyo, 192-0397 Japan

** Department of Electrical Engineering and Computer Science, Tottori University, 4-101 Koyama-Minami, Tottori, 680-8552 Japan

Abstract

Prediction and measurement of temperature fields formed by a small heat source inside liquid are important for various thermal applications such as inductive heating of magnetic particles, crystal growth, laser heating, etc. However, as local temperature differences cause natural convection in many cases, the temperature field becomes complicated, which makes the prediction and measurement more difficult. We thus used the temperature imaging method based on the temperature dependence of the absorption band of water in the near-infrared region to investigate the temperature field around a 1-mm-diameter magnetic sphere under induction heating. Furthermore, to construct a quantitative model of natural convection around the heated sphere, the flow field was measured using particle tracking velocimetry with Kalman filter simultaneously with the temperature field.

KEY WORDS: Temperature field, Near-infrared absorption imaging, Natural convection, Particle tracking velocimetry

1. Introduction

When there is uneven density due to temperature and concentration in fluid, a flow called natural convection is caused by the difference in body force acting on the fluid. In the case of natural convection due to heat, when the heating element starts generating heat and its temperature rises, the heat is first conducted to the fluid by thermal conduction. Since the fluid near the object that is influenced by the temperature rise has a smaller density than the fluid part at a greater distance, it receives buoyancy according to Archimedes' principle and starts the upward movement. Because of this natural convection, the range of heat transfer is limited to a close area of the heating element, and the movement of the fluid is also the cause of the density difference. The expansion of the velocity field along the surface of the heating element is also limited to a certain area [1].

It is significant for heat and mass transfer studies and applications using small heat sources that natural convection and temperature fields are visualized and measured. Compared to theoretical studies, experimental ones addressing natural convection fields near heat sources are limited because of difficulties in measuring the temperature and flow velocity distributions. For the measurement inside liquid, techniques without probe using interferometry, microwave, radiometry and ultrasound have been developed. However, a temperature solution of sub-Kelvin or a spatial resolution of sub-millimeter, both of which are needed for the natural convection research, cannot be obtained by any technique.

This paper presents a near-infrared (NIR) imaging system that simultaneously measures the temperature and flow fields formed by a 1-mm-diameter steel sphere. The temperature is based on the temperature dependence of an NIR absorption band of water [2, 3], Using this NIR-based technique with the Inverse Abel Transform (IAT) [4], we got absorbance difference images of water around the steel sphere and then estimated the temperature distribution. The flow visualization and velocity measurement are implemented by particle tracking velocimetry (PTV) [5].

2. Method

2.1 Temperature dependence of NIR absorption band of water

Figure 1 (a) shows the absorption spectra of water at temperatures from 16.0°C to 44.0°C in 4.0°C increments in a wavelength range from 1100 nm to 1250 nm. The optical path length was 10.0 mm. The water temperature was controlled by a Peltier heating/cooling device. Using the measured light intensity transmitted through the water cell, I , and the incident light intensity, I_0 , which was measured beforehand using the empty cell, the absorbance, A , was determined by:

$$A = -\log_{10}\left(\frac{I}{I_0}\right). \quad (1)$$

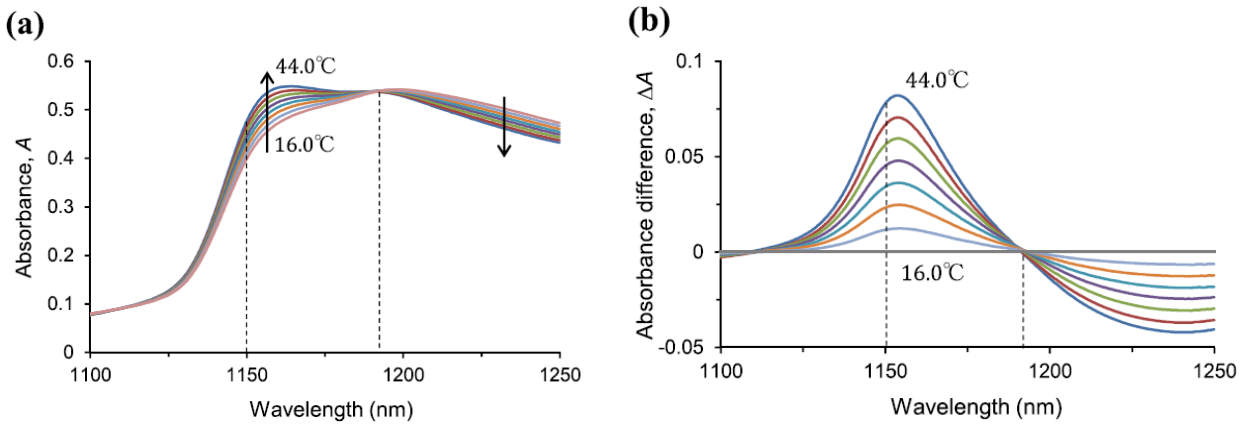


Fig. 1: (a) Absorbance spectra of water from 16.0 °C to 44.0 °C in 4.0 °C increments. The optical path length is 10.0 mm. (b) Absorbance difference spectra. The absorbance at 16.0 °C is the reference. Reproduced from Ref. 4.

In Fig. 1 (a), the absorption band of water, called the $\nu_1 + \nu_2 + \nu_3$ band [3], is observed and its spectrum depends on the temperature. Figure 1 (b) presents the difference spectra, ΔA , defined as:

$$\Delta A = A - A_r = -\log_{10}\left(\frac{I}{I_0}\right) + \log\left(\frac{I_r}{I_0}\right), \quad (2)$$

where I_r is the light intensity at the reference condition (16.0 °C here). It is found that A at around a wavelength (λ) of 1150 nm increases the most as the temperature increases and the isosbestic point, at which A does not depend on the temperature, exists at $\lambda = 1193$ nm. There is a good linear relationship between A and temperature at $\lambda = 1150$ nm. μ is defined as:

$$\mu = \frac{A}{d} \quad (3)$$

where d is the light path length.

In this study, the light beam at $\lambda = 1150$ nm was incident on a water layer, and two-dimensional (2D) projection images, i.e., I images, in which μ corresponding to temperature along the optical path in water was integrated, were acquired. From the I images, the ΔA images are obtained by Eq. (2). Then, as described later, it is possible to estimate the temperature distributions in water from the ΔA images.

2.2 Experimental setup

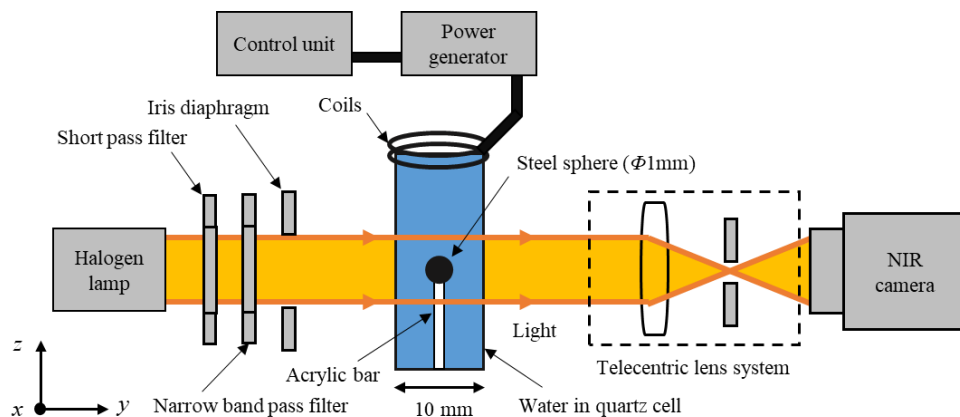


Fig. 2: experimental setup

Figure 2 shows a schematic of the experimental setup. Since a sample thickness of 10 to 200 mm is suitable for measurement in the wavelength region of the 1100 nm wavelength band, a cell with an optical path length of 10 mm was used. Using a coil (25 mm in diameter, 2 turns) connected to a heating device (SPW 900/56, CEIA), perform induction heating of the chromium steel sphere. The position of the coil is about 12 mm from the magnetic sphere, the frequency at heating is 760 kHz, the maximum output power was 5.6 kW, and the output can be adjusted with a duty ratio of 10-99%. The light from the halogen lamp pass through a short pass filter ($\lambda < 1300$ nm), and then passed through a narrow bandpass filter at $\lambda = 1150$ nm with a full width at half maximum of 10 nm. After that, transmitted light is irradiated to the cell through the diaphragm. The light transmitted through the sample is detected by near infrared cameras (Alpha NIR, FLIR) through a telecentric lens. The detector of the camera is an InGaAs array of 320 (H) \times 256 (V) with the wavelength sensitivity range of 800–1700 nm and the output of 12-bit digital data. In order to obtain the temperature and flow velocity fields simultaneously, we added hollow-glass tracer particles with the diameter range of 9–13 μm (1001443, Lavision GmbH, Germany) to the water. Two or three drops of a 0.8 g/L particle suspension solution were put and stirred in the water. The two-dimensional particle tracking velocimetry (2D-PTV) based on binary correlation method is used to measure the velocity distribution.

2.3 Inverse Abel transform and multi-Gaussian approximation

The near infrared absorption spectrum of water has a temperature dependence [2, 3], and the absorption coefficient μ of the $\nu_1 + \nu_2 + \nu_3$ absorption band existing near $\lambda = 1150$ nm changes depending on the temperature. Therefore, temperature information can be obtained by measuring the absorbance A by irradiating the measurement target with light of a wavelength with high temperature sensitivity in the band. In actual measurement, the absorbance difference ΔA between A and the reference absorbance A_r is determined as the equation (2). Since A is an integrated quantity of μ along the optical path, assuming that the light traveling direction is y , the following equation can be formed.

$$\Delta A = \int \Delta \mu dy \quad (4)$$

The temperature distribution around the heated sphere is expected to be spherically symmetric in the time when heat conduction is dominant. At this time, the following Abel transformation holds between the line profiles $\Delta A(r')$ and $\Delta \mu(r)$ extracted from the $\Delta A(x, z)$ image [3].

$$\Delta A(r') = 2 \int_{r'}^R \frac{r \Delta \mu dr}{\sqrt{r^2 - r'^2}} \quad (5)$$

Where r is the distance from the center of the heated sphere in three-dimensional space ($r = \sqrt{x^2 + y^2 + z^2}$), r' is the distance from the center of the heated sphere in the two-dimensional image ($r' = \sqrt{x^2 + z^2}$), R is the radius of the measurement area, when $r \geq R$, $\Delta \mu(R) = 0$. The Abel inverse transform of $\Delta A(r')$ is

$$\Delta \mu(r) = -\frac{1}{\pi} \int_r^R \frac{d\Delta A(r')}{dr'} \frac{dr'}{\sqrt{r'^2 - r^2}} \quad (6)$$

In this study, the Abel inverse transform of the Gaussian function can be analytically determined, and the multi-Gaussian function fits well to monotonically decreasing data as in the case of heat conduction from a single heat source. The approximation method is adopted as following equation.

$$\Delta A(r') = \sum_{j=1}^N a_j \left\{ \exp\left(-\frac{r'^2}{\sigma_j^2}\right) - \exp\left(-\frac{R^2}{\sigma_j^2}\right) \right\} \quad (7)$$

The inverse Abel transform of Eq. (5) is

$$\Delta \mu(r) = \sum_{j=1}^N \frac{1}{\sqrt{\pi}} \frac{a_j}{\sigma_j} \left\{ \exp\left(-\frac{r^2}{\sigma_j^2}\right) \operatorname{erf}\left(\frac{\sqrt{R^2 - r^2}}{\sigma_j}\right) \right\} \quad (8)$$

where a_j is a weighting factor and σ_j is a dispersion parameter.

$$\Delta T = \frac{\Delta\mu}{a} \quad (9)$$

3. Results and discussion

3.1 Temperature difference

Figure 3 presents the acquired $\Delta A(x, y)$ images at $t = 0.99$ s and 1.65 s for the heating power levels of 50% and 80%. The increases in ΔA near the sphere are clearly observed in the four images. It is reasonable that at $t = 1.65$ s for 80%, the increasing area is the largest. The distributions of ΔA are circular symmetric with respect to the center of the sphere because, within this period ($t < 1.65$ s), thermal conduction was predominant while little significant natural convection occurred. In these ΔA images, the tracer particles can be observed as high ΔA dots. To these circular symmetric ΔA distributions, the inverse Abel transform as described above can be applied. Figure 4 shows the radial temperature difference profile determined by the inverse Abel transform. The temperature distribution was able to catch the temperature rise properly without being affected by the tracer particles. For 80% in Fig. 4, large temperature gradients causing large heat conduction in the r -direction were observed near the magnetic sphere. It was confirmed that the temperature rise becomes larger as the heating power level becomes larger.

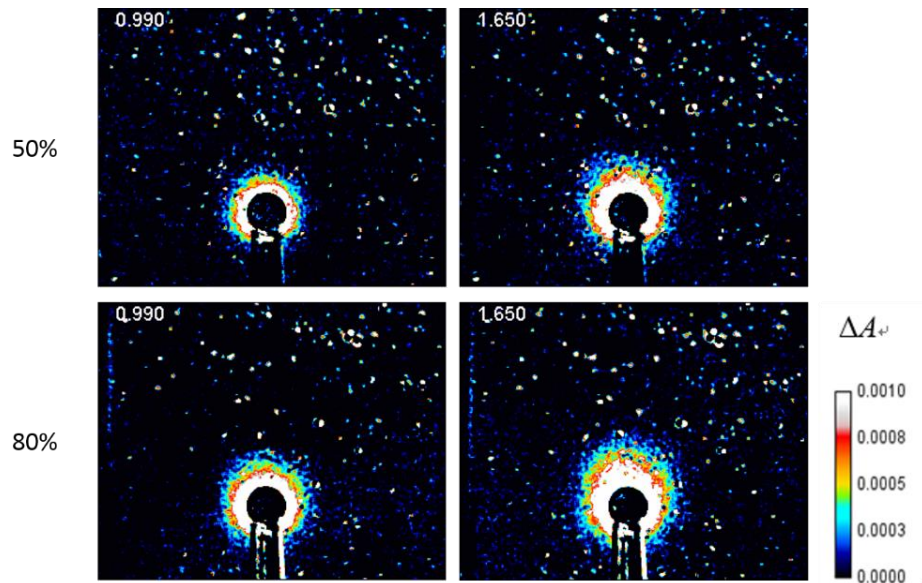


Fig. 3: Images of ΔA at $\lambda = 1150$ nm at $t = 0.99$ s (left) and 1.65 s (right) for the heating power levels of 50 % and 80 %.

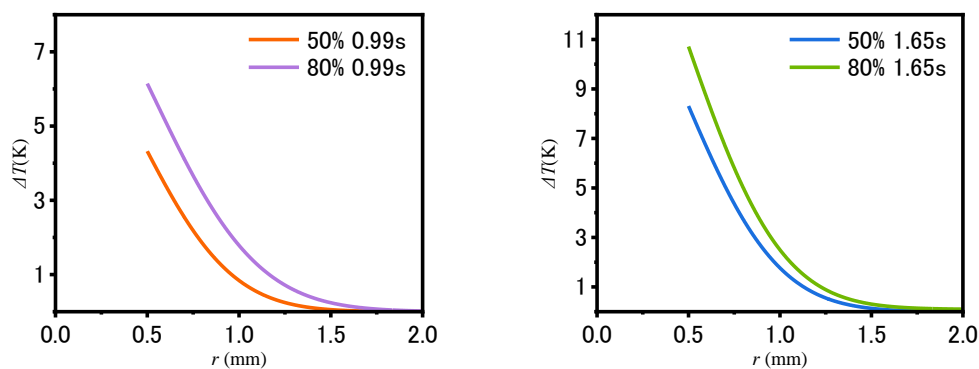


Fig. 4: Temperature difference profiles in the radial direction $t = 0.99$ s and 1.65 s for the heating power levels of 50% and 80%.

3.2 Particle tracking

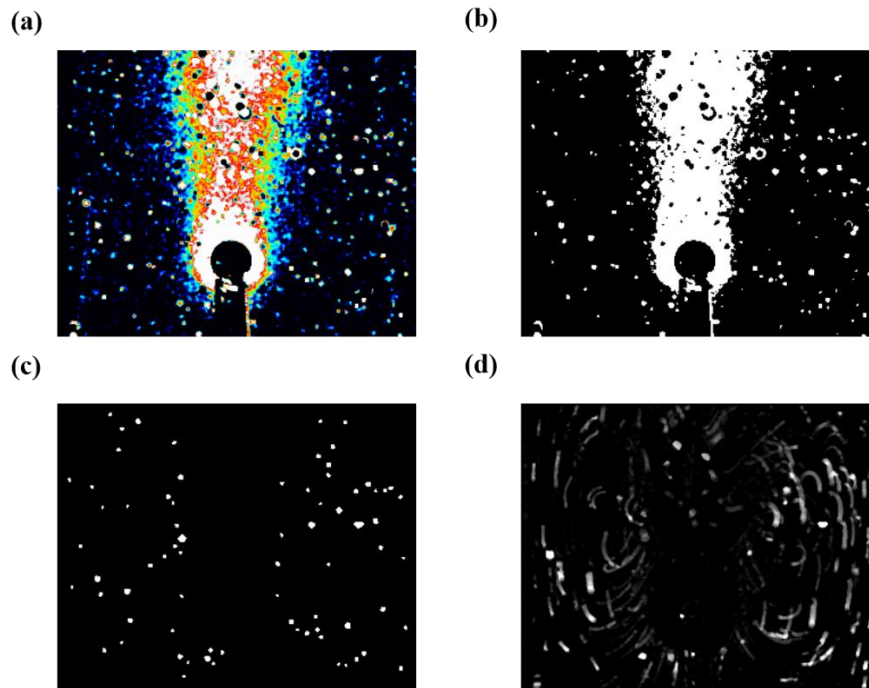


Fig. 5: Particle tracking procedure for analyzing the movement of the particles. (a) Image of ΔA . (b) Banarized image of ΔA . (c) Extraction of the positions of particles. (d) Using Kalman filter in series of images, the streaks of particles are defined

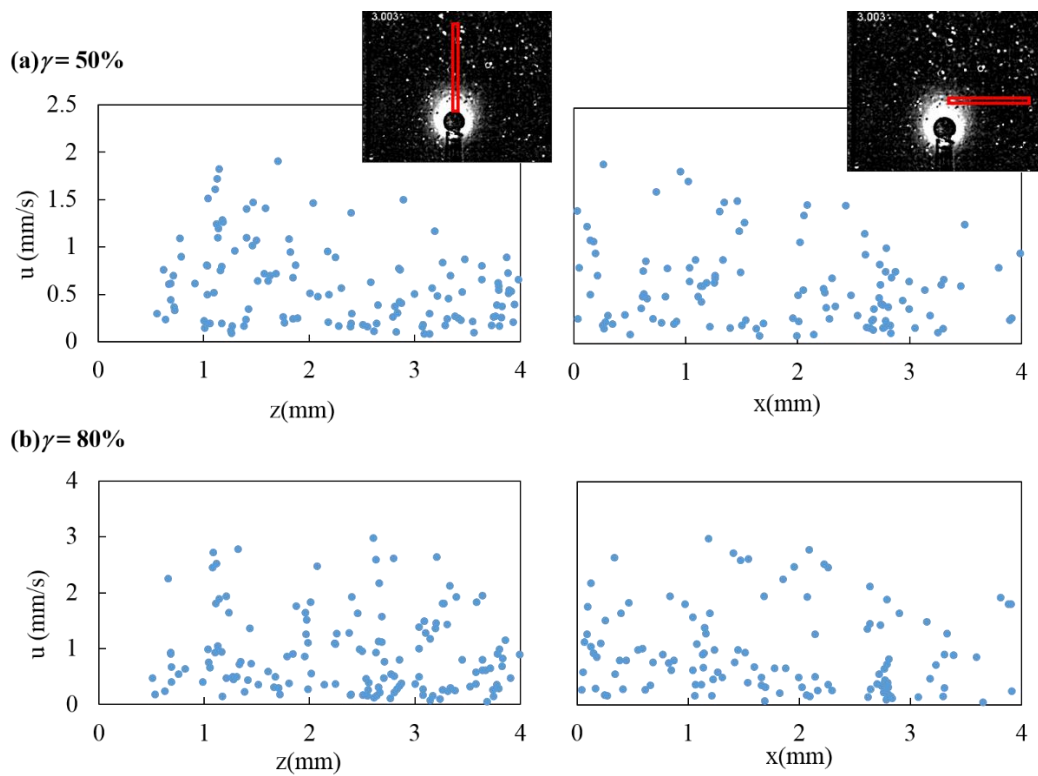


Fig. 6: Plots of the z component of the particle velocity, u , at $t = 3.0$ s in the upper region indicated as the red-line rectangle in the inset image (left) and in the horizontal region at $z = 1$ mm (right).

The following image processing was implemented to recognize particles in the ΔA images. As shown in Fig. 5, in the first step, each ΔA image was binarized with a threshold of 3.0×10^{-4} . Next, the higher ΔA region (white part in the image) caused by the temperature increase was filtered out with area threshold of 50 pixels. Third, to reduce the noises in the ΔA image, the white regions with a circularity of 0.85 to 1.00 were selected. Finally, applying Kalman filter [6] to the series of images, the streaks of particles are obtained.

Figure 6 shows the z component of the particle velocity, u , estimated by the PTV. Although substantial variations in the plots are observed, it is found that in the left graph of Figure 6 (a) u at z from 1 to 1.5 mm is the largest in the upper region. In the right two graphs in Fig. 6, as x increases, u seems to slightly decrease; however, this trend is not significant because of transmission imaging by which all particles along the light path direction is detected. On the other hand, it is clear, by comparison between Fig. 6 (a) and (b), that the heating power largely affects the free convection strength; the biggest u values for $\gamma = 80\%$ are about 1.5 times larger than those for $\gamma = 50\%$. To reveal the 3D flow field, particle identification from the two-directional imaging must be achieved, which is a challenge for future research.

4. Conclusion

Simultaneous measurement of temperature and particle tracing was performed using near infrared temperature imaging method and PTV. Even when the tracer particles are stirred in water, a clear rise in absorbance is seen with the rise in temperature, indicating that the rise in temperature is detected. However, in the case that the particles existed in the high ΔA region above the heated sphere, it was difficult to detect these particles using the PTV method based on the binary method. On the other hand, the application of the PTV with Kalman filter to the absorbance images provided the streaks of particles, leading to the estimation of flow velocity.

REFERENCES

- [1] T. Nishiyama, Fluid Dynamics, Nikkan Kogyo Shimbun; 1971. (in Japanese)
- [2] N. Kakuta, K. Kondo, A. Ozaki, H. Arimoto, and Y. Yamada, "Temperature imaging of sub-millimeter-thick water using a near-infrared camera", International Journal of Heat and Mass Transfer. 2009:52:4221-4228.
- [3] N. Kakuta, Y. Fukuhara, K. Kondo, H. Arimoto, and Y. Yamada, Temperature imaging of water in a microchannel using thermal sensitivity of near-infrared absorption, Lab Chip. 2011:11:3479-3486.
- [4] N. Kakuta, K. Nishijima, K. Kondo, and Y. Yamada, Near-infrared measurement of water temperature near a 1-mm-diameter magnetic, Journal of Applied Physics. 2017:122:44901-10
- [5] The Visualization Society of Japan, PIV Handbook. Morikita Publishing; 2018. (in Japanese)
- [6] Kalman, R. E., A new approach to linear filtering and prediction problems, Transaction of the ASME Journal of Basic Engineering, 1960:35-45.